Materials Horizons

Accepted Manuscript

This article can be cited before page numbers have been issued, to do this please use: L. Tang, L. Mou, J. Shang, J. Dou, W. Zhang and X. Jiang, *Mater. Horiz.*, 2020, DOI: 10.1039/C9MH01761E.

ROYAL SOCIETY OF CHEMISTRY

rsc.li/materials-horizons

View Article Online
DOI: 10.1039/C9MH01761E

In this article, we introduce the metal-hygroscopic polymer conductors (MHPC) that can secrete liquid metal solders for reliable connections with rigid electronics in large deformations. Just like biological system that can respond to external stimulus, our MHPC will become conductive and secrete solders in response to change of humidity. We believe that liquid metal particles within conductors will break, merge into conductive paths, and erupt from the surface due to shrinkage and swelling of coated polymers in response to the change of humidity. The MHPC also has a comparable stretrchablility with the most stretchable reported conductors. Based on the secreted solders, we redesign connections between conductors and electronics. Electronics can be stably connected on soft conductors by pressure; no extra solder, solvent, or heat is needed. Such connections demonstrate both high electrical and mechanical robustness under large deformations. As a result, we create a stretchable system that can mechanically support and electrically connect rigid electronics to substitute the conventional printed circuit boards.

View Article Online
DOI: 10.1039/C9MH01761E

ARTICLE

Metal-hygroscopic Polymer Conductors that Can Secrete Solders for Connections in Stretchable Devices

Lixue Tang[a, c], Lei Mou[a, c], Jin Shang[a, c], Jiabin Dou[a, c], Wei Zhang[a, c], and Xingyu Jiang[a, b, c *]

Received 00th January 20xx,
Accepted 00th January 20xx

DOI: 10.1039/x0xx00000x

Wearable electronics have great potential to enable seamless human-machine interfaces and can dramatically improve the quality of life by using advanced monitoring and therapeutic devices. Despite great progress in wearable devices, very few wearable devices can be both highly integrated and stretchable (strain>100%) due to the lack of reliable connections between the soft conductors and rigid electronics. Here, we report the highly stretchable metal-hygroscopic polymer conductors that can secrete solders for connections. Propelled by changing humidity, liquid metal particles within conductors will merge and erupt, providing electrical connections for electronics, while the coated adhesive can provide mechanical connections. Thus rigid electronics can be stably connected on conductors by pressure; no extra solder, solvent, or heat is needed. Those stable connections and high stretchability of conductors (10^5 S/m at a strain of 800%) allow integrated electronics to stretch to a strain of 150%. We created a stretchable, integrated device that is double-sided and multi-layered such that it can sense oxygen saturation in blood, heart rate, strain and temperature.

Introduction

Stretchable circuits have great potential in wearable/implantable devices[1-7], soft robotics[8-10], and human-machine interfaces[11, 12]. Fabricating stretchable conductors has been one of the most important parts for realizing stretchable circuits[13-25], because currently it is impossible to avoid using rigid electronics in a functional circuit. To achieve stretchable circuits, stretchable conductors are used to substitute the rigid interconnects (Cu) on conventional printed circuit board (PCB). Though there are many strategies for making stretchable conductors, one current challenge is to achieve stable connections between the soft conductors and the rigid electronics during deformations. Recently, wavy-structured metal has been adopted to build stretchable circuits for complicated functions[13, 14], however, wavy structure cannot be directly applied to current design for PCB and using wavy structure alone cannot resolve connections between layers, all interconnects and through-holes need to be re-designed to ensure the stretchability and make full use of the space on the substrate. Also, the fabrication of such wavy structure is costly and complicated. Directly printing elastic ink on substrates can be straightforward and cost-competitive strategies to fabricate stretchable circuits with similar interconnects layout as conventional PCB. The reported elastic ink for printing stretchable electronics including nanoscale metals[4,15,16] and/or liquid-metal[17-23], usually have ultra-high stretchability (200%-1000%), but those inks cannot reliably connect with rigid electronics particularly under stretch. To achieve stretchable circuits with complicated functions, it is also important to form both electrical and mechanical connections between different sides and different layers[24, 25].

Here, we report metal-hygroscopic polymer conductors (MHPC) that can secrete solders for rigid electronics to connect. We utilized the environmental humidity[26,27] to make the MHPC conductive permanently and form liquid metal solders (LMS) on the surface for electrical connections. Combining with the pressure-sensitive adhesives (PSA), and vertical interconnect accesses (VIAs) on the substrate, we developed the printed circuit adhesive tapes (PCAT) to substitute the conventional PCB for stretchable devices to overcome the challenges in connections including double-sided connections, multi-layered connections and connections with rigid electronics. The layout of interconnects in our MHPC-based system can be the same as that of conventional PCB, thus without changing the layout of an existing circuit, we can turn most PCB (even if they are double-sided and multi-layered) into stretchable circuits.

Based on the MHPC, we developed electric devices that contain different number of PCAT layers, each layer can be patterned with just one side or both sides. We fabricated an oximeter containing one PCAT layer which demonstrates high robustness under large deformations (150% strain). We created

[a] Beijing Engineering Research Center for BioNanotechnology and CAS Key Laboratory for Biomedical Effects of Nanomaterials and Nanosafety, CAS Center for Excellence in Nanoscience, National Center for NanoScience and Technology, No. 11 Zhongguancun Beiyitiao, Beijing 100190, P. R. China
[b] Department of Biomedical Engineering, Southern University of Science and Technology, No. 1088 Xueyuan Rd, Nanshan District, Shenzhen, Guangdong 518055, P. R. China
[c] University of Chinese Academy of Sciences, 19 A Yuquan Road, Shijingshan District, Beijing, 100049, P. R. China
* Corresponding author, E-mail: jiang@sustech.edu.cn
Electronic Supplementary Information (ESI) available: [details of any supplementary information available should be included here]. See DOI: 10.1039/x0xx00000x

View Article Online
DOI: 10.1039/C9MH01761E

an integrated stretchable system containing three PCAT layers that can conformably attach to the skin and monitor oxygen saturation in blood (SpO2), heart rate, strain and temperature.

Results and discussion

The MHPC

We sonicate liquid metals in the hygroscopic polymer solution to fabricate the MHPC ink (Figure S1a (i)). Here, we choose the low-cost and biocompatible Gallium-indium alloy as the liquid metal[28,29] and the PVP (Polyvinyl pyrrolidone, a pharmaceutical additive with high levels of biocompatibility) as the hygroscopic polymer.

We change the humidity to merge liquid metal particles within MHPC. There are many strategies to sinter the LM particles including freezing, strains, and the use of tips to draw conductive path on deposit particles[19-22, 30-32], however, none of those can provide both electrical and mechanical connections for electronics. We use a cost-competitive strategy, screen printing, to pattern the MHPC (Figure 1a and figure S1a (ii)). The MHPC are not conductive after printing because a thin, dense, and non-conductive oxide layer (thickness: ~0.5-3 nm) will form on the surface of liquid metal[33]. The continuous protective oxide film will also prevent the further oxidation of the liquid metal particles. We adjust the humidity to make the MHPC conductive (Figure S1a (iii)).The MHPC will keep conductivity permanently under ambient conditions. Meanwhile, promoted by the humidity change, some liquid metals will erupt from the conductor and form LMS on the surface of the MHPC (Figure 1a and figure S1b). We believe that the polymers on the liquid metal particles will shrink when the humidity changes from high to low. The squeezed liquid metal particles will break and form conductive paths between the particles. Those conductive paths will not disappear after the humidity treatment under ambient conditions, thus the MHPC will obtain a permanent conductivity. During shrinkage, some squeezed liquid metals will erupt from the defects on the PVP membrane and form the LMS. Figure 1b illustrates the water adsorption and desorption process of the coated polymer when adjusting the humidity of the atmosphere around the MHPC.

We conduct the wet (RH=100%)-dry (RH=4.5%) cycles to the MHPC for conductance and scanning electron microscope (SEM) characterization. To characterize the conductive paths within the MHPC, we dissolve the hygroscopic polymers within MHPC in different phases in water before characterizations. The real morphology of the MHPC surface at different phases are shown in figure S2a. Figure 1c presents the conductance changes during 3 wet-dry cycles. After printing, the MHPC is non-conductive (phase I), the liquid metal particles within the MHPC present a round and isolated morphology (Figure 1d (I)). The MHPC is an insulator during the first step of humidification. The exposure of the liquid metal to water only last for dozens of seconds. The short-time exposure to water will have ignorable influence on the liquid metal particles due to the low reaction rate between the gallium and water in room temperature[34, 35]. We place the humidified MHPC in a dry environment (RH=4.5%), after drying for about 2 mins, the conductance will increase sharply and finally reach a stable value to allow the MHPC to become a conductor. Liquid metal particles within MHPC become wrinkled and interconnected ((Figure 1d (II), phase II) due to the shrinkage of the PVP. We believe that liquid metal particles are squeezed by contracted polymers, thus thin oxide layer on particles will be broken and conductive paths will form between particles. In the second cycle, the conductance slightly decreased during humidification, we believe that the coated polymers will swell in wet environment, and the squeezed liquid metal particles will relax. The established conductive paths will not disappear, but their width will decrease, causing a decrease in conductivity of MHPC (figure S2b). Similar to the first cycle, the conductance will increase after drying for about 2 mins and reach phase III. Compared with phase II, liquid metal particles at phase III have more and wider conductive paths (Figure 1d (III)). The increase in wet-dry cycles can increase the number and width of the conductive paths. After the third cycle, the increase of the conductance is not remarkable. Most particles nearly merged together (phase IV). With the increase of the wet-dry cycles, the MHPC will become thinner and flatter because of the shrinkage of the polymer and the eruption of the LMS (Figure 1e and figure S4).

The MHPC have different conductivity when drying in different humidity. We conduct 5 wet-dry cycles to the MHPC in different humidity (Figure 1f). The conductivity of the MHPC will increase with the cycles and tend to be a constant after 3 cycles. We found that lower RH lead to higher conductivity of the MHPC. We believe polymers within the MHPC shrink greater in lower humidity. We measure the shrinkage of the hygroscopic polymer in different humidity. To exclude the influence of the liquid metal particles, we directly screen print the polymer solution on silicone, thus the shrinkage of the polymer in different humidity can be reflected by the curvature of polymer coated silicon strips (Figure S3). From figure S3c and figure 1f, we found that PVP-coat silicone strips have larger curvature when drying in lower humidity, which suggest that PVP shrinks to a greater extent in lower humidity. we know that when the humidity for the drying process is lower than or equal to 38% RH, the curvature of the PVP-coat silicone strips will be larger than 0.2 mm^{-1}, and the MHPC will become conductive after the first wet-dry cycle.

The performances of the MHPC are influenced by polymers, solvents and the diameter of the liquid metal particles. The hygroscopic polymers are necessary in the MHPC ink though they are present in low proportions (~1.25%, wt. %). We tested MHPC ink that contains hygroscopic polymers with five different concentrations (Figure 1g). The MHPC is non-conductive after wet-dry cycles when the concentration of the PVP is under 0.5%. However, MHPC has the best performance in conductivity when containing 1.25% PVP. The excess addition of polymers (>2.5%) will cause the isolation of particles by polymers, leading to the decrease of conductivity. We found that most hygroscopic polymers such as PVP, polyethylene oxide (PEO), and hydroxypropyl methylcellulose (HPMC) can make MHPC inks while non-hygroscopic polymers such as thermoplastic polyurethane (TPU) and ethylene-vinyl acetate copolymer (EVA) cannot function (Figure S5b). Compared with organic solvents, waterborne solvents can improve the conductivity of the MHPC at each wet-dry cycle (Figure S5c, S5d), because the evaporation of waterborne solvents after

View Article Online DOI: 10.1039/C9MH01761E

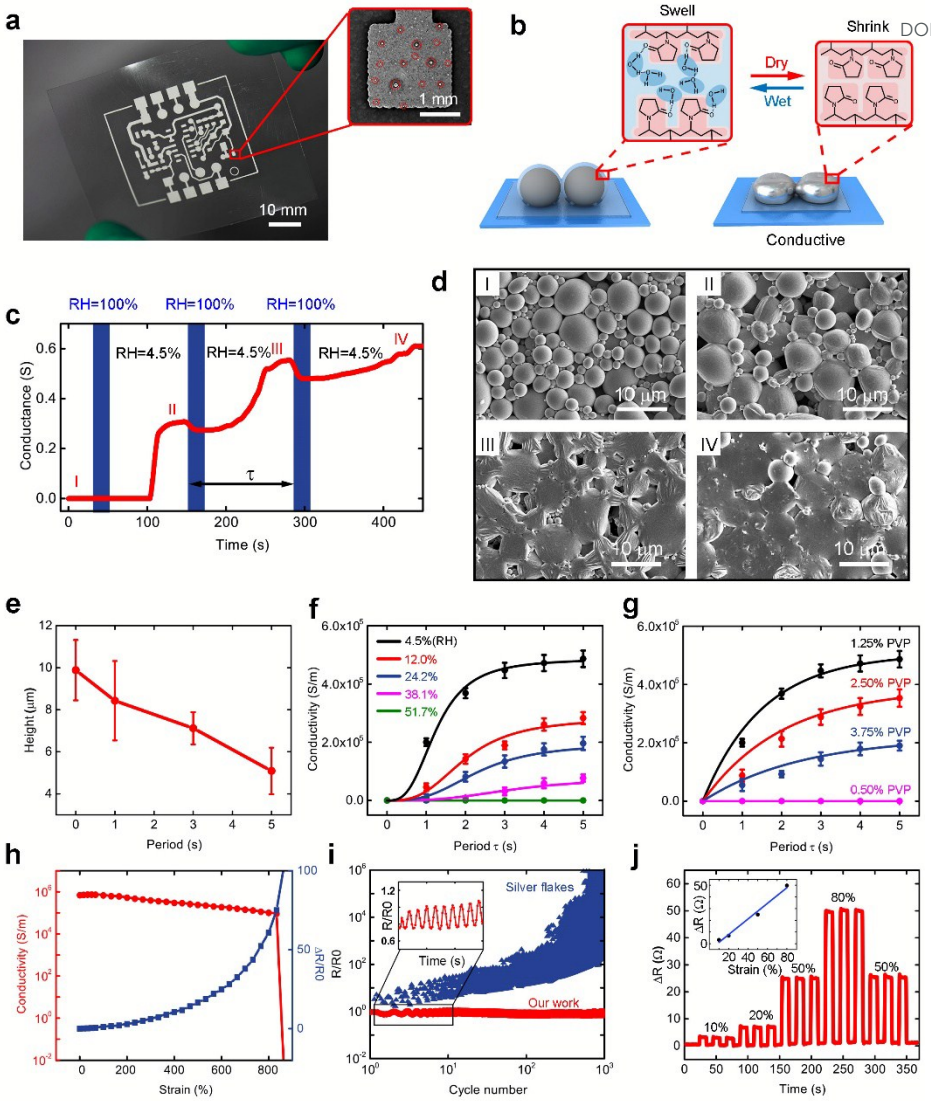

Figure 1. Characterization of the MHPC. (a) Optical image of the printed MHPC, inset, magnified optical image of the MHPC with LMSs (dashed circles) on the surface. **(b)** Illustration of the water adsorption process. **(c)** The change in conductance of the MHPC as a function of wet-dry cycles, τ, one wet-dry cycle. **(d)** SEM characterization of the MHPC after different wet-dry cycles which corresponds to phase I to IV in (c). **(e)** Thickness of the MHPC depends on the wet-dry cycles applied on MHPC. **(f)** Conductivity of the MHPC depends on wet-dry cycles under different humidity. **(g)** Conductivity of the MHPC with different concentrations (0%, 0.5%, 1.25%, 2.5%, 3.75%, wt. %) of hygroscopic polymer depends on wet-dry cycles. **(h)** The conductivity and change in resistance of MHPC versus different tensile strains. **(i)** A comparison in repeatability of this work to silver flake inks[15,16] (stretching from 0% to 50% for 1000 cycles). **(j)** Real-time resistance monitoring of the serpentine-structured MHPC in different strains, inset, the change in resistance of the MHPC sensor versus different strains. Error bars in this paper represent standard error.

printing equal a wet-dry process. The diameter of the particles is sonication time dependent (Figure S6b). MHPC with small particles (<1 μm) is an insulator after 5 wet-dry cycles. The SEM shows that the cycles do not change the morphology of particles (Figure S6a). We believe that breaking liquid metal particles with smaller diameters requires larger external stress[21] which exceeds the stress that the polymer can offer when shrinking.

The MHPC has excellent stretchability. After 3 wet-dry cycles, the MHPC has conductivity of $6.9*10^5$ S/m at initial length. When we gradually stretch the MHPC to a strain of 800%, it keeps a high conductivity about $1.0*10^5$ S/m (Figure 1h), which is comparable to most conductors with the top stretchability[21,23]. The change in resistance is also slight (<1.0) when the strain is lower than 100% (Figure 1h).

The MHPC also presents an excellent repeatability when we stretched the MHPC from a strain of 0% to 50% for 1000 cycles (Figure 1i). After stretchy cycles the change in resistance of MHPC is negligible. In comparison, under the same conditions, reported elastic conductors based on silver flakes[15,16] become almost an insulator. Based on its good repeatability and stretchability, the MHPC can be printed to serpentine structures as strain sensors. The MHPC strain sensors (Figure S7) have a large range of repeatability (up to 80%) (Figure 1j). In this range, the change in resistance is

View Article Online
DOI: 10.1039/C9MH01761E

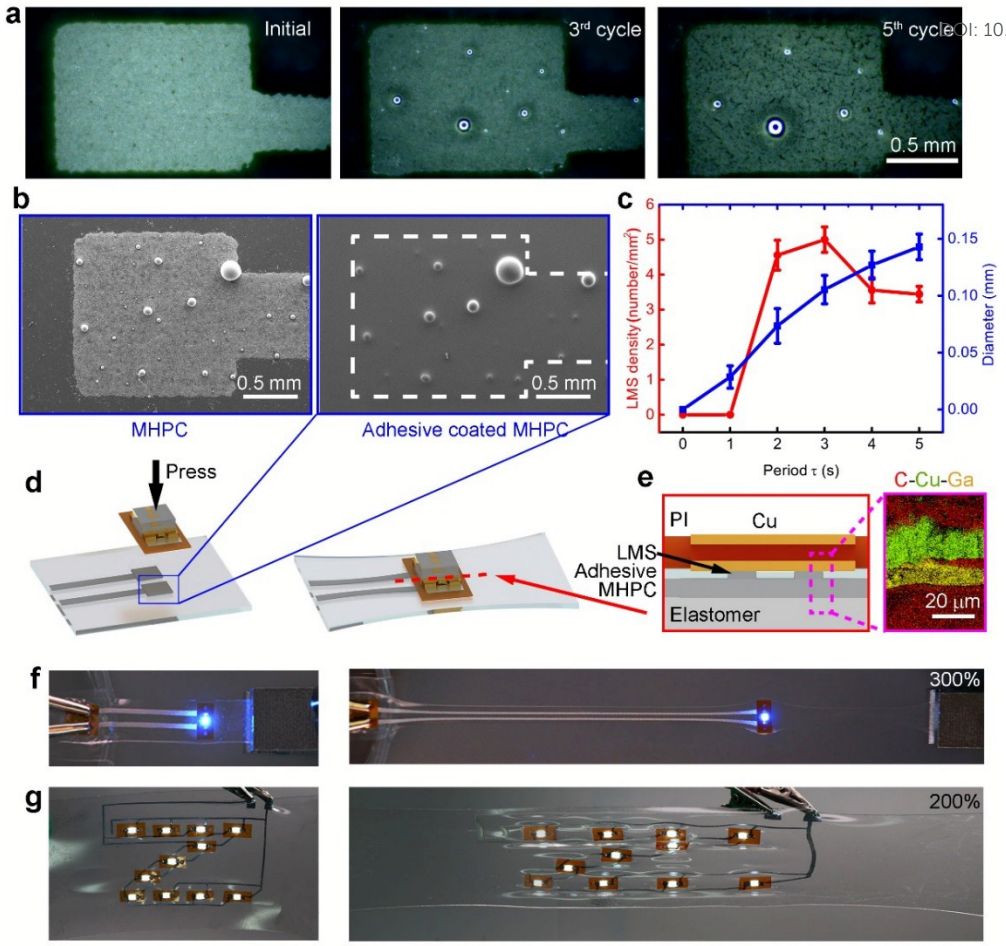

Figure 2. Characterization and stretching of the PCAT. (a) Optical image of the MHPC after different wet-dry cycles **(b)** SEM characterization of the MHPC before **(left)** and after **(right)** the coat of PSA. **(c)** Numbers and diameter (the largest one) of the LMSs depends on the wet-dry cycles. **(d)** Illustration of the connections of ECEs on the PCAT. **(e)** Cross-section of the cuts defined by the dashed lines in (c), left, the illustration, right, the EDS analysis. **(f)** A stretchable LED circuit in a tensile strain of 300%. **(g)** A stretchable LED array in a tensile strain of 200%.

nearly linear with the strain, and the coefficient of variation of the resistance at the strain of 50% is less than 1.5%.

To ensure a stable performance of the MHPC, we sealed the MHPC after desirable wet-dry cycles to isolate from water. Once the MHPC is sealed by Ecoflex, the liquid metal is isolated from water, and will not be oxidized by oxygen or hydrolyzed by water. Thus, the MHPC will maintain a predictable electrical performance.

The excellent stretchability and repeatability of the MHPC ensures the reliability of the MHPC-based stretchable system. During deformations, the changes in resistance of interconnects are negligible and predictable, thus we developed robust interconnects for the stretchable system.

The soft/rigid connections

The PCAT can provide stable soft/rigid connections due to LMS and the PSA. During wet-dry cycles, the shrinkage of the PVP membrane caused by humidity change will not only merge liquid metal particles, but also drive some merged liquid metals to erupt from the coated PVP membranes, forming LMS on the surface of MHPC (Figure 2a, figure S8 and Figure S9). We coat a thin layer of PSA on the PCAT which can provide mechanical connection for rigid electronics. The density and the diameter of the LMS are dependent on wet-dry cycles. We only count the LMS whose diameter are larger than 50 μm, because those LMS will not be insulated by the coated adhesive (Figure 2b, 2c). LMS will thrive at the first 3 cycles. The LMS will absorb liquid metals from the MHPC to increase both in quantity and size, making the MHPC thinner and flatter (Figure S4). However, with the increase of the cycles, the largest LMS will absorb liquid metals from smaller LMS, causing the disappearance of some smaller LMS (Figure 2a, and figure S8). Thus the density of the LMS will decrease after 3 cycles (Figure 2c). To ensure both good conductivity and sufficient LME on the conductors, we carried out 3 wet-dry cycles to the MHPC for connections. After connections, the MHPC need to be sealed to isolate from vapours.

Electronics can form stable electrical and mechanical connection with the PCAT by press (Figure 2d). We connect the rigid electronics with copper patterned polyimide film to obtain the

View Article Online
DOI: 10.1039/C9MH01761E

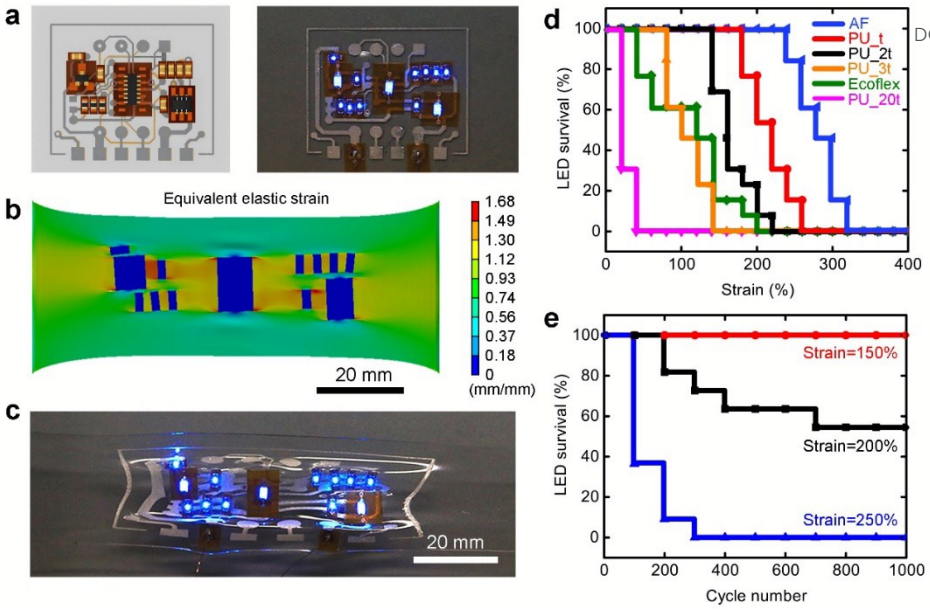

Figure 3. Simulation of the PCAT-based oximeter. (a) Illustration of the double-sided oximeter (left) and a LED circuit to simulate the electrical connection of the stretchable oximeter. **(b)** FEA results of strain distribution on the device under a tensile strain of 100%. **(c)** The simulated LED circuit in deformations. **(d)** LED survival ratio of the LED circuit in (c) depends on different strains. **(e)** LED survival ratio depends on different cycles. Thickness, PU-t, 0.01mm; PU-2t, 0.02 mm; PU-3t, 0.03 mm; PU-20t, 0.20 mm, AF and Ecoflex, 0.20 mm.

electric connection elements (ECEs). Polyimide film can form more robust connection with the PSA due to the larger contact area and stronger van der Waals force than the rigid electronics. The peel strength of the pressure sensitive adhesive between the polyimide and the polyurethane is 13.2±1.86 N/cm (180 degree peel method, figure S10a). Also, the ECEs can enlarge the contact pads between electronics and MHPC, thus enough LMS will form to ensure stable electrical connections. Figure 2e and figure S10b shows the cross-section of the ECEs connected PCAT, it demonstrates that LMS will break the isolation of adhesive and form connections with the copper on the ECEs. The ECEs are commercially available, any PCB manufacturer can produce ECEs in a large quantity if the circuit designs are offered (Figure S11, S12).

We tested the robustness of ECEs connected on the PCAT. The circuit that contains one LED can be easily stretched to a strain of 300% (Figure 2f). The circuit that contains LED array can be stretched to a strain of 200%, all LEDs can connect firmly with the conductors (Figure 2g). However, it will be different for integrated functional circuits because such circuits usually have electronics with different sizes and uneven distributions.

To demonstrate that our MHPC on the PCAT can provide reliable connections for integrated functional circuits, we study the robustness of an oximeter which contains one PCAT layer through mechanical simulation and LED simulation.

Based on the PCAT, we fabricate a stretchable oximeter using the conventional PCB design. The oximeter is double-sided which contains one PCAT layer with MHPC interconnects on both sides (Figure 3a left). Our stretchable oximeter can still function after stretching and releasing from a strain of 150% (Figure S13). This stretchable device can be stretched for more than 1000 cycles at a strain of 80% (Figure S14) which demonstrates the high robustness and reliability.

From the mechanical simulation, strains/stress tend to concentrate around the ECEs when the device is being stretched (Figure 3b). When the force applied on the adhesives exceed the peel stress of the adhesives, the PCB polyimide will detach from the elastomer. The simulation also shows an uneven strain distribution on the PCAT, when 100% strain is applied, the deformation on some area of the PCAT will exceed 150%, luckily, interconnects on such area can still keep high conductivity.

We used a LED circuit to simulate the oximeter. The LED circuit has the same layout of ECEs as the oximeter, we will know the states of each ECE during stretching by directly observing the LEDs (Figure 3a right and 3c). We gradually applied strains on the circuit from 0% to 400% to test how many LEDs can survive (keep function) during deformations. We use different elastomers with different thickness to conduct the LED simulation. We found that thinner and softer substrate can make a more stretchable device. At the same thickness, PCAT with softer substrate can be stretched to a larger strain until the first failure of the connected ECE. The acrylic foam (AF) is much softer than polyurethane (PU, PU-20t) at the thickness of 0.2 mm (Figure S15), as a result, the AF-based stretchable circuit lost its first LED at the strain of 220%, and gradually lost all the LEDs until the strain reaches about 300% (Figure 3d and figure S16). By contrast, the PU-based PCAT (PU-20t) lost LEDs at the strain of 10%. We used polyurethane with different thickness to demonstrate that stretchable circuits with thinner substrate have better performance in stretchability (figure 3d). We found that in stretchable circuit with a 0.01 mm PU substrate, some of LEDs became disconnected at the strain of 180%, and gradually all LEDs became disconnected until the strain reaches about 260%. By contrast, the stretchable circuit with a 0.2 mm PU nearly lost its stretchability, some of LEDs become disconnected at

View Article Online
DOI: 10.1039/C9MH01761E

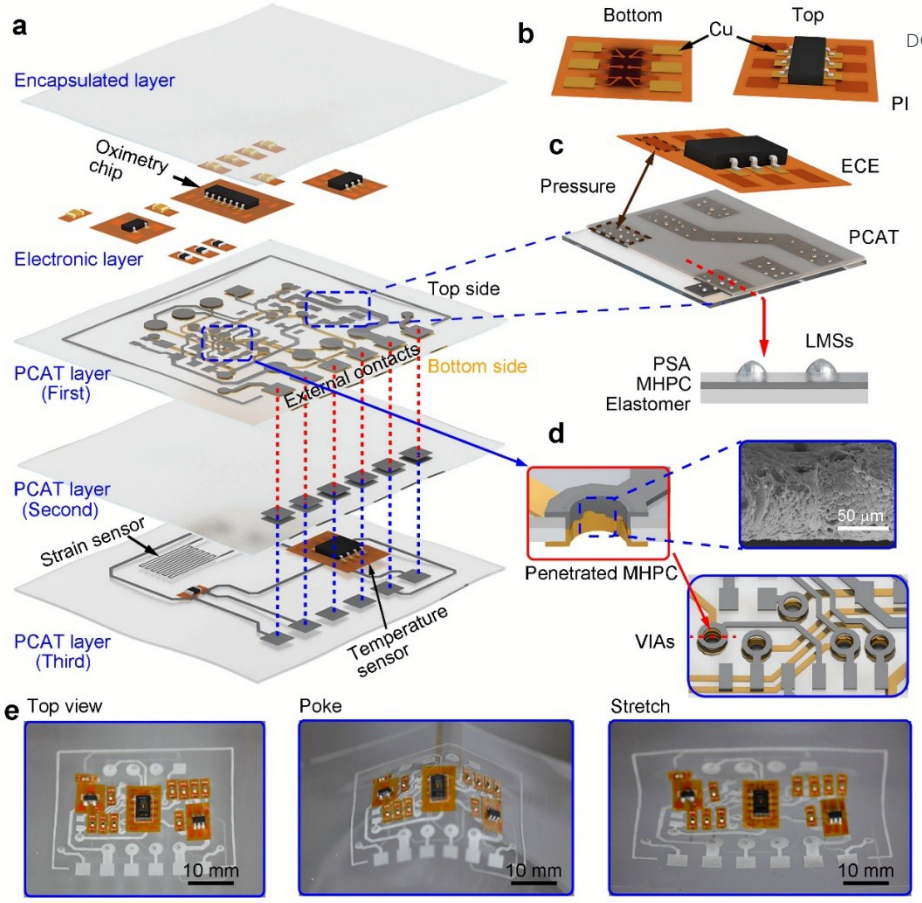

Figure 4. Schematic illustrations and optical image of the PCAT based and multi-layered stretchable system. (a) Exploded schematics of the stretchable system that integrated oximeter, strain and temperature sensor. **(b)** Illustrations of the top and back side of the ECE. **(c)** Illustrations of the PCAT that contains the substrate, the MHPC, the coated PSA and extruded LMSs; inset, cross-sectional diagrams of the cuts defined by the dashed lines. **(d)** Illustration of VIAs on the PCAT, inset, illustrations show that the MHPC on top and back side of the substrate will form electrical connections through the penetrated MHPC. **(e)** Optical image of the stretchable system on the top view when freestanding (left), poked (middle), and stretched at a 50% strain (right).

the strain of 10%. From the mechanical simulation, we found that thinner substrate can lead to smaller stress on the ECEs (Figure S17).

We also adopt the soft silicone Ecoflex, which has similar strain-stress curve to the AF, as the substrate. However, the silicone-based circuit has poor performance (~40%) in stretchability (Figure 3d), because the PSA have low affinity with the elastomer, adhesives will detach from the substrate when stretched.

To obtain stretchable devices with better stretchability, we should use softer and thinner substrates and enhance the affinity between the substrate and the ECEs.

To test the repeatability of the system, we stretched the AF-based LED circuits for 1000 cycles in different strains. We found that all the ECEs in the circuit can still function at a strain of 250% in the first cycle, however, with the increase of cycles, all ECEs will lose connections with the PCAT at about 300 cycles (Figure 3e). At a strain 150%, all ECEs function even after 1000 cycles which demonstrate that our stretchable oximeter is robust and reliable below a strain of 150% which can be suitable for functioning in the most active part of the body such as wrists, knuckles and knees.

The integrated stretchable devices

To demonstrate the multi-layered PCAT circuits, we fabricate the double-sided and multi-layered stretchable systems based on the MHPC. Figure 4a shows the structure and the circuit design of the integrated stretchable system. The stretchable system contains five layers including three PCAT layers, one encapsulation layer, and the electronic layer. The layout of MHPC interconnects and the electric components is the same as that of conventional PCB. The PCAT layers can provide both electrical and mechanical connections for electronics (Figure 4b and 4c). The first and third PCAT provide connections for electronics while the second PCAT serves to insulate and connect different layers. The encapsulation layer is responsible for isolating the MHPC from vapours which may affect the performances of MHPC. Different electric components are welded on polyimide film to fabricate into different ECEs. Those ECEs can directly connect with the PCAT by gentle pressure due to the LMS and PSA.

View Article Online
DOI: 10.1039/C9MH01761E

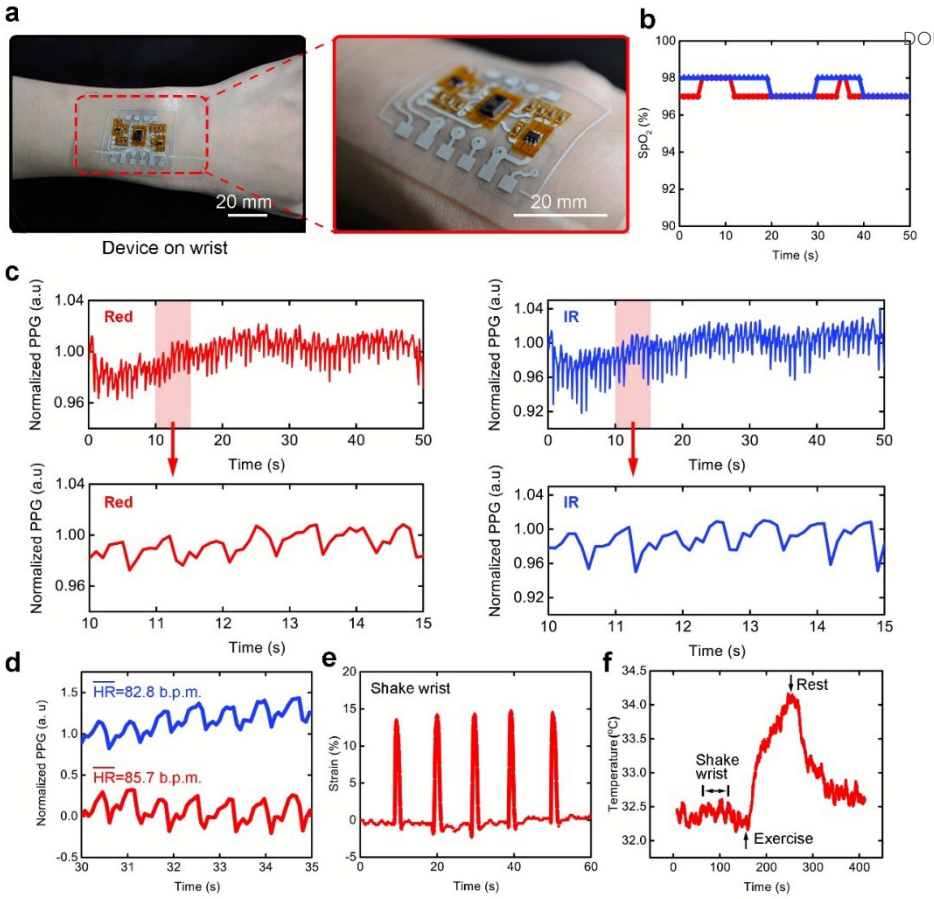

Figure 5. Stretchable system on wrist for detection. (a) Optical image of the stretchable system attached on wrist when shaking wrist. **(b)** Measured SpO_2 using rigid PCB-based oximeter (blue) and stretchable PCAT-based device (red) **(c)** The red and infrared photoplethysmography (PPG) signals acquired from the PCAT-based oximeter to calculate the SpO_2. (Top) A 50 s sequence. (Bottom) Zoomed-in data during 10 s<t <15 s shows the red channel **(left)** and IR (Infrared Red) channel **(right)**. **(d)** PPG signals measured to show the heartbeat using rigid PCB-based oximeter (blue), and PCAT-based device (red). Data are plotted in arbitrary units, normalized and offset in the vertical direction to facilitate comparisons. **(e)** Measured bending strain corresponding to repeated wrist shaking. **(f)** Measured skin temperature change corresponding to exercise and rest.

The double-sided PCAT is based on VIAs distributed on the PCAT (Figure 4d). Different from the current VIA techniques, we drill holes on the substrate first (Figure S18a). After the alignment, we screen print the MHPC interconnects on one side. During printing, the MHPC ink will enter the through-holes due to the capillarity force. The penetrated distance depends on the diameter of the holes, and smaller diameters lead to large penetrated distance due to a larger capillarity force (Figure S19). After printing MHPC interconnects on the other side, the penetrated MHPC from either side will meet in the hole and form vertical electrical access between different sides (Figure 4d, figure S18b and figure S18c). Compared with reported double-sided circuits[24,25], we do not need to fill the holes with conductive fillings one by one, VIAs will automatically form after printing which dramatically simplified the fabrication of double-sided circuits. We also test the electrical-mechanical performance of MHPC printed on both sides of the substrates connected by VIAs, we found that VIAs will not affect the stretchability and repeatability of the MHPC (Figure S20). Based on the double-sided PCAT circuits, we can turn most of the functional circuits into stretchable devices since the double-sided circuit is the most widely used PCB option.

Using double-sided and multi-layered PCAT, we can achieve circuits with multiplex functions that were previously impossible using single-layered circuits. Figure 4e shows the overall sizes of the stretchable devices which are about 50*40*2 (L*W*T) mm^3. The integrated stretchable system is an extension of the oximeter in figure 4 which contains an oximeter on the first PCAT layer, a strain sensor and a temperature sensor on the third PCAT layer, and a thin Ecoflex encapsulated layer. The design of each layer are shown in Figure S21 and Figure S22. This system demonstrated high robustness under 50% strains (Figure 4e), which is beyond the typical strain of skin.

We attached the stretchable systems on the wrist to monitor the SpO_2 and heart rate. Based on the same circuit layout, a PCB-based oximeter was fabricated by PCB manufacturer as a comparison, the only difference is that the size of the layout in PCAT is enlarged so that sufficient LMS can form on the MHPC contact pads to form electrical connections with ECEs. Through the analysis of Arduino, SpO_2 can be obtained from the PPG signals (light absorption) at two

different wavelengths (red 660 nm and Infrared red 880 nm). We attach the PCAT-based oximeter on the wrist for a 50-seconds measurement. The measured oxygen saturation varied from 97%-98% which has the same performance as the PCB-based rigid devices. The PPG signals in red channel and IR channel are shown in figure 5c. Each peak in signals are distinguishable. We can calculate the heart rate according to the peaks in PPG signals. PPG signals and calculated heart rate from the red channel show almost identical results for both PCAT-based oximeter and PCB-based oximeter. Here, an error of 3.5% in heat rate is seen between the two different oximeters (Figure 5d). One obvious advantage of the stretchable PCAT-based oximeter is that it can directly attach to the skin and comfortably worn to achieve functions due to its good stretchability. By contrast, the rigid PCB-based oximeter needs external supports to firmly attach to the skin.

We attached the integrated system on the wrist to monitor the skin strains and temperature. The system can be attached to the skin (Figure 5a) and shows good repeatability when monitoring the strain on the shaking wrist (Figure 5e). We attached the system on the wrist for temperature sensing. The temperature increases rapidly when exercising and drops after rest. The strains arising from shaking wrist have negligible influence on temperature monitoring (Figure 5f). This integrated device achieves a stretchability about 50% (Figure 1g and figure S23). Compared with the oximeter that contains one PCAT layer, the stretchability of the integrated device is compromised, but it is still beyond the typical deformations of skin (~20%). Increasing the number of PCAT layer will sacrifice the stretchability of the devices, because it equals increasing the thickness of the PCAT which will decrease the stretchability of the PCAT as we have discussed in figure 4. If we continue to increase the PCAT layer, the integrated system will eventually lose the stretchability. However, our integrated system containing three PCAT layer can satisfy requirements of most devices.

Conclusions

We have developed a stretchable MHPC-based system for fabricating a highly stretchable, robust and reliable double-sided and multi-layered circuits. We overcome the difficulties in stretchable devices that connections failure will happen in deformations, thus electric devices based on our system can make full use of the stretchability of conductors. We can design a stretchable circuit based on conventional PCB layout or directly converting most conventional PCB-based circuits, even if they are double-sided and multi-layered, into stretchable devices without changing their original interconnects layout. The electronics based on our system should have large contact pads to generate sufficient LMSs to reliably connect with the electronics. In the future, we will increase the density of the LMS on the MHPC, thus devices can be fabricated smaller and lighter. Our system also have great potential in implantable electronics which are vulnerable to high temperature and organic solvents, because electrical and mechanical connections in our system can be achieved by pressures, no heat, solvent or extra solder is needed.

Conflicts of interest

There are no conflicts to declare.

View Article Online
DOI: 10.1039/C9MH01761E

Acknowledgements

We thank the National Key R&D Program of China (2017YFA0205901), the National Natural Science Foundation of China (21535001, 81730051, 21761142006) and the Chinese Academy of Sciences (QYZDJ-SSW-SLH039, 121D11KYSB20170026, XDA16020902) for financial support.

Notes and references

1 Q. Zhai, S. Gong, Y. Wang, Q. Lyu, Y. Liu, Y. Ling, J. Wang, G. P. Simon, W. Cheng, *ACS Appl. Mater. Interfaces* 2019, **11**, 9724.
2 Y. Lu, K. Jiang, D. Chen, G. Shen, *Nano Energy*, 2019, **58**, 624.
3 D.-H. Kim, N. Lu, R. Ghaffari, Y.-S. Kim, S. P. Lee, L. Xu, J. Wu, R.-H. Kim, J. Song, Z. Liu, J. Viventi, B. Graff, B. Elolampi, M. Mansour, M. J. Slepian, S. Hwang, J. D. Moss, S.-M. Won, Y. Huang, B. Litt, J. A. Rogers, *Nat. Mater.* 2011, **10**, 316.
4 S. Choi, S. I. Han, D. Jung, H. J. Hwang, C. Lim, S. Bae, O. K. Park, C. M. Tschabrunn, M. Lee, S. Y. Bae, J. W. Yu, J. H. Ryu, S.-W. Lee, K. Park, P. M. Kang, W. B. Lee, R. Nezafat, T. Hyeon, D.-H. Kim, *Nat. Nanotechnol.* 2018, **13**, 1048.
5 L. Li, Z. Lou, D. Chen, K. Jiang, W. Han, G. Shen, *Small* 2018, **14**, 1702829.
6 J. Y. Oh, S. Rondeau-Gagné, Y.-C. Chiu, A. Chortos, F. Lissel, G.-J. N. Wang, B. C. Schroeder, T. Kurosawa, J. Lopez, T. Katsumata, J. Xu, C. Zhu, X. Gu, W.-G. Bae, Y. Kim, L. Jin, J. W. Chung, J. B.-H. Tok, Z. Bao, *Nature* 2016, **539**, 411.
7 Y. Zhao, Q. Zhai, D. Dong, T. An, S. Gong, Q. Shi, W. Cheng, *Anal. Chem.* 2019, **91**, 6569.
8 J. Wu, S. -Y. Tang, T. Fang, W. Li, X. Li, S. Zhang, *Adv. Mater*. 2018, **30,** 1805039.
9 M. Wehner, R. L. Truby, D. J. Fitzgerald, B. Mosadegh, G. M. Whitesides, J. A. Lewis, R. J. Wood, *Nature* 2016, **536,** 451.
10 E. J. Markvicka, M. D. Bartlett, X. Huang, C. Majidi, *Nat. Mater*. 2018, **17**, 618.
11 M. Han, H. Wang, Y. Yang, C. Liang, W. Bai, Z. Yan, H. Li, Y. Xue, X. Wang, B. Akar, H. Zhao, H. Luan, J. Lim, I. Kandela, G. A. Ameer, Y. Zhang, Y. Huang, J. A. Rogers, *Nat. Electron.* 2019, **2**, 26.
12 L. Tian, B. Zimmerman, A. Akhtar, K. J. Yu, M. Moore, J. Wu, R. J. Larsen, J. W. Lee, J. Li, Y. Liu, B. Metzger, S. Qu, X. Guo, K. E. Mathewson, J. A. Fan, J. Cornman, M. Fatina, Z. Xie, Y. Ma, J. Zhang, Y. Zhang, F. Dolcos, M. Fabiani, G. Gratton, T. Bretl, L. J. Hargrove, P. V. Braun, Y. Huang, J. A. Rogers, *Nat. Biomed. Eng.* 2019, **3**, 194.
13 S. Xu1, Y. Zhang, L. Jia, K. E. Mathewson, K.-I. Jang, J. Kim, H. Fu, X. Huang, P. Chava1, R. Wang, S. Bhole, L. Wang, Y. J. Na, Y. Guan, M. Flavin, Z. Han, Y. Huang, J. A. Rogers, *Science* 2014, **344**, 70.
14 Z. Lou, S. Chen, L. Wang, R. Shi, L. Li, K. Jiang, D. Chen, G. Shen, *Nano Energy*, 2017, **38**, 28.
15 N. Matsuhisa, M. Kaltenbrunner, T. Yokota, H. Jinno, K. Kuribara, T. Sekitani, T. Someya, *Nat. Commun.* 2015, **6**, 7461.
16 N. Matsuhisa, D. Inoue, P. Zalar, H. Jin, Y. Matsuba, A. Itoh, T. Yokota, D. Hashizume, T. Someya. *Nat. Mater.* 2017, **5**, 1.
17 Y. Zheng, Z.-Z. He, J. Yang, J. Liu, *Sci. Rep.* 2014, **4**, 4588.
18 M. D. Dickey, *Adv. Mater.* 2017, **29**, 1606425.
19 M. G. Mohammed, R. Kramer, *Adv. Mater.* 2017, 29, 1604965.

View Article Online
DOI: 10.1039/C9MH01761E

20 L. Tang, S. Cheng, L. Zhang, H. Mi, L. Mou, S. Yang, Z. Huang, X. Shi, X. Jiang, *iScience* 2018, **4**, 302-311.
21 L. Tang, L. Mou, W. Zhang, X. Jiang, *ACS Appl. Mater. Interfaces* 2019, **11**, 7138.
22 H. Wang, Y. Yao, Z. He, W. Rao, L. Hu, S. Chen, J. Lin, J. Gao, P. Zhang, X. Sun, X. Wang, Y. Cui, Q. Wang, S. Dong, G. Chen, J. Liu, *Adv. Mater*. 2019, **31**, 1901337.
23 J. Wang, G. Cai, S. Li, D. Gao, J. Xiong, P. S. Lee, *Adv. Mater*. 2018, **30**, 1706157.
24 Z. Huang, Y. Hao, Y. Li, H. Hu, C. Wang, A. Nomoto, T. Pan, Y. Gu, Y. Chen, T. Zhang, W. Li, Y. Lei, N. Kim, C. Wang, L. Zhang, J. W. Ward, A. Maralani, X. Li, M. F. Durstock, A. Pisano, Y. Lin, S. Xu, *Nat. Electron*. 2018**, 1**, 473.
25 D. G. Marques, P. A. Lopes, A. T. D. Almeida, C. Majidi, M. Tavakoli, *Lab Chip* 2019, **19**, 897.
26 B. Shin, J. Ha, M. Lee, K. Park, G. H. Park, T. H. Choi, K.-J. Cho, H.-Y. Kim, Sci. Robot. 2018, 3, eaar2629.
27 J. Zhou, C. Wu, D. Wu, Q. Wang, Y. Chen, *Chem. Commun*. 2018, **54**, 11610.
28 J. Yan, Y. Lu, G. Chen, M. Yang, Z. Gu, *Chem. Soc. Rev*. 2018, **47**, 2518-2533.
29 J. Yan, X. Zhang, Y. Liu, Y. Ye, J. Yu, Q. Chen, J. Wang, Y. Zhang, Q. Hu, Y. Kang, M. Yang, Z. Gu, *Nano Res.* 2019, **12**, 1313.
30 J. Park, H. S. Kang, J. Baek, T. H. Park, S. Oh, H. Lee, M. Koo, C. Park, *ACS Nano* 2019, 13, 9122
31 S. Chen, H. Wang, X. Sun, Q. Wang, X. Wang, L. Chen, L. Zhang, R. Guo, J. Liu, *Mater. Horiz.* 2019, **6**, 1854.
32 A. Fassler, C. Majidi, *Adv. Mater*. 2015, 27, 1928.
33 N. Kazem, T. Hellebrekers, C. Majidi, *Adv. Mater*. 2017, **29**, 1605985
34 X. Li, M. Li, L. Zong, X. Wu, J. You, P. Du, C. Li, *Adv. Funct. Mater*. 2018, **28**, 1804197.
35 M. R. Khan, C. Trlica, J. So, M. Valeri, M. D. Dickey, *ACS Appl. Mater. Interfaces* 2014, **6**, 22467.